

# Pump Electron-Positron Pairs from Well Potential

Qiang Wang,<sup>1</sup> Jie Liu,<sup>1,2</sup> and Li-Bin Fu<sup>1,2,\*</sup>

<sup>1</sup>*National Laboratory of Science and Technology on Computational Physics,  
Institute of Applied Physics and Computational Mathematics, Beijing 100088, China*

<sup>2</sup>*HEDPS, Center for Applied Physics and Technology, Peking University, Beijing 100871, China  
and IFSA collaborative Center of MoE College of Engineering, Peking University, Beijing 100871, China*

In this paper we show that electron-positron pairs can be pumped inexhaustibly with a constant production rate from the one-dimensional well potential with oscillating depth or width. Bound states embedded in the Dirac sea can be pulled out and pushed to the positive continuum, become scattering states. Pauli block, which dominant the saturation of pair creation in the static super-critical well potential, can be broken by the ejection of electrons. We find that the width oscillating mode is more efficient than the depth oscillating mode. In the adiabatic limit, pair number as a function of upper boundary of the oscillating, will reveal the diving of the bound states.

PACS numbers: 03.65.Pm, 12.20.-m, 02.60.-x

## I. INTRODUCTION

Since Einstein's relativistic theory tell that the matter can convert into energy, the possibility of converting energy into matter, i.e., the electron-positron pair, as predicted by Dirac in quantum electrodynamics [1], has attracted a great deal of interest[2]. In presence of a static and uniform electric field, the quantum electrodynamic (QED) vacuum may break down and decay into electron-positron pairs due to a quantum tunneling effect [4–6]. The critical Schwinger field is  $E_c = m^2 c^3 / (|e| \hbar)$ , which can accelerate the electron to an energy of the order of its rest mass on its Compton wavelength  $\lambda_C = \hbar/mc$ , where  $m$  is the electron mass. Starting from the works of Brezin and Popov et.al [7–9], the Schwinger mechanism was generalized to time dependent fields [10–17], where another mechanism may be responsible for the pair creation. If the frequency of the alternating field exceeds the gap  $2mc^2$ , electrons in Dirac sea can transit to positive states and pairs are triggered. Experimentally, pairs can be generated by the relativistic heavy-ion collisions[18] or the collision of an intense laser pulse and a 46 GeV electron beam[19], but pairs created from pure laser light has not been observed until now.

Recently, various numerical approach were developed to deal with the time dependent Dirac equation[20–22], the Klein paradox[23, 24], the Zitterbewegung[25], and the pair production process [26–31]. The one-dimensional well potential, specially, for its simplicity, is studied extensively[27–29, 32, 33]. The super critical well potential has bound states embedded in the negative continuum can cause spontaneous electron-positron pair creation. Theoretical investigations are expected to make the physics of the creation clear and predict a higher generation rate. However, The Pauli exclusion principle will block further creation once the bound

states are occupied, resulting a asymptotic saturation behavior[27, 28, 33]. Motivated by this requirement and a better understanding of the pair creation process in the one-dimensional well potential, we examine the pair creation in a well with its width or depth oscillating. By oscillating the width and depth, the transfer channels for population are opened and closed alternately. The electrons confined in the well will be released and the Pauli block become invalid. This can lead to a non-vanishing production rate, which means that pairs can be pumped inexhaustibly from the well.

This paper is organized as follows. In Sec.II we present the model and the numerical method we employed. The well potential is set to be oscillating in two modes, the width oscillating mode and the depth oscillating mode. The energy spectrum is plotted as a function of the width or the depth. In Sec.III. we discuss the pair production process in both two modes. The time evolution of pair number, spacial density and pumping rate are studied. We also investigate the adiabatic limit of the oscillating. In the last section we give a brief summary.

## II. MODEL AND METHOD

### A. Model: one-dimensional well potential with oscillating depth or width

In one dimension, the time evolution of the Heisenberg field operator  $\hat{\Psi}(z, t)$  is given by the Dirac equation (without spin, for simplicity in this paper) [34]

$$i \frac{\partial}{\partial t} \hat{\Psi}(z, t) = [c \sigma_1 \cdot \hat{p}_z + c^2 \sigma_3 + V(z, t)] \hat{\Psi}(z, t). \quad (1)$$

$\sigma_1, \sigma_3$  are Pauli matrices,  $c$  is the speed of light in vacuum,  $V(z, t)$  is the external potential. The atomic units ([a.u.]) is used in this paper:  $m = \hbar = e = 1$ ,  $c = 1/\alpha \approx 137.0359991$ ,  $\alpha$  is fine-structure constant, Compton wave length of electron is  $\lambda_C = 1/c$ . The Hamiltonian of the

\* lbfu@iapcm.ac.cn

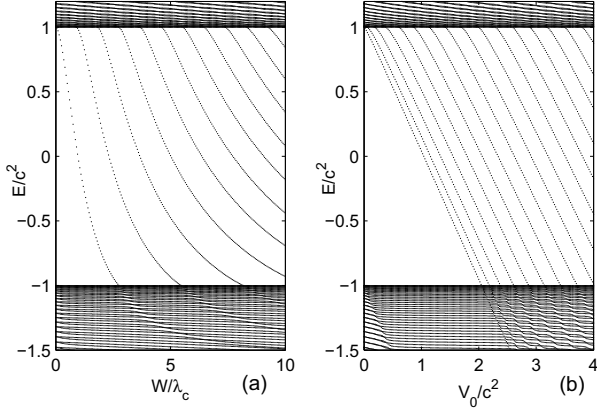


Figure 1. The energy spectrum of the total Hamiltonian as a function of the width or the depth of the potential. (a),  $V_0 = 2.53c^2$ , as  $W$  increasing, the bound states dive into the Dirac sea at  $W = 2.79, 5.51, 8.21, \dots$  (in units of  $\lambda_C$ , the electron Compton wavelength). (b),  $W = 10\lambda_C$ , as  $V_0$  increasing, the bound states dive into the Dirac sea at  $V_0 = 2.05, 2.19, 2.38, 2.62, 2.87, 3.15, 3.43, 3.73, \dots$  (in units of  $c^2$ ).

system is  $H = [c\sigma_1 \cdot \hat{p}_z + c^2\sigma_3 + V(z, t)]$ . We define the potential as

$$V(z, t) = \frac{V_0(t)}{2} \left[ \tanh\left(\frac{z - \frac{W(t)}{2}}{D}\right) - \tanh\left(\frac{z + \frac{W(t)}{2}}{D}\right) \right]. \quad (2)$$

$D$  is the width of potential edge (a measure of the width of the electric field), and we set  $D = 0.3\lambda_C$ . The numerical box size is set to  $L = 2.5$ .

The potential width  $W(t)$  and the depth  $V_0(t)$  (positive, but note that the potential  $V(z, t)$  is negative in the center and zero elsewhere) are set to two modes: (1) the **W-oscillating mode**:  $V_0$  is constant,  $W(t) = W_1 + \frac{1}{2}(W_2 - W_1)[1 + \sin(\omega_W(t) - \pi/2)]$ ; (2) the **V-oscillating mode**:  $W$  is constant,  $V_0(t) = V_1 + \frac{1}{2}(V_2 - V_1)[1 + \sin(\omega_V(t) - \pi/2)]$ . In this paper we assume  $W_1 = 0$  and  $V_1 = 0$ , then  $W(t)$  (or  $V_0(t)$ ) varies as a sine function between zero and its upper boundary  $W_2$  (or  $V_2$ ), and the turning on process is from zero point with first order derivative equal to zero. In the following numerical simulation, we choose the total evolution time to be the period ( $T_W$  or  $T_V$ ) of the oscillating  $W(t)$  or  $V(t)$  multiples an integer, to make the potential turning off is finished with first order derivative equal to zero.

The numerically energy spectrum of the total Hamiltonian of finite-size (length, for one dimension) are presented in Fig. 1 for varying  $W$  and  $V_0$ , which can be a schematic of the real one-dimensional system. In Fig. 1, we show the critical width or depth, and the behavior of 'diving' of the bound states into the negative continuum. For example, if  $V_0 = 2.53c^2$ , there are bound states embedded and then pair can be spontaneously triggered only when  $W > 2.79\lambda_C$ .

## B. Method: the numerical quantum field theoretical approach

In recent years, numerical quantum field theoretical approach [31] has been established to overcome the single particle picture described by quantum mechanics and the mathematical difficulty of quantum electrodynamics. In this section we will briefly review this method and describe that how do we deal with the model in this paper.

The field operator can be expressed in terms of the electron annihilation and positron creation operators as [31]

$$\hat{\Psi}(z, t) = \sum_p \hat{b}_p W_p(z, t) + \sum_n \hat{d}_n^\dagger W_n(z, t) \quad (3)$$

$$= \sum_p \hat{b}_p(t) W_p(z) + \sum_n \hat{d}_n^\dagger(t) W_n(z), \quad (4)$$

in which  $W_{p(n)}(z) = \langle z | p(n) \rangle$  is the solution of the filed-free Dirac Hamiltonian ( $V(z, t) = 0$ ),  $W_{p(n)}(z, t) = \langle z | p(n)(t) \rangle$  is the time dependent solution of the Dirac equation (1), and the term  $\sum_{p(n)}$  denotes the summation over all states with positive (negative) energy. The eigenstates of the filed-free Hamiltonian are

$$W_p(z) = \frac{e^{ipz}}{\sqrt{4\pi E}} \begin{bmatrix} \sqrt{E+c^2} \\ \text{sign}(p) \sqrt{E-c^2} \end{bmatrix} \quad (5)$$

$$W_n(z) = \frac{e^{inz}}{\sqrt{-4\pi E}} \begin{bmatrix} -\text{sign}(n) \sqrt{-E-c^2} \\ \sqrt{-E+c^2} \end{bmatrix}, \quad (6)$$

where  $E_p = \sqrt{c^4 + p^2 c^2}$ , and  $E_n = -\sqrt{c^4 + n^2 c^2}$  respectively. The time dependent single particle wave function  $W_{p(n)}(z, t)$  can be got by introducing the time-evolution operator  $\hat{U}(t_2, t_1) = \hat{T} \exp\left(-\frac{i}{\hbar} \int_{t_1}^{t_2} dt' \hat{H}(t')\right)$ ,

$$W_{p(n)}(z, t) = \hat{U}(t, t=0) W_{p(n)}(z), \quad (7)$$

where  $\hat{T}$  denotes the Dyson time ordering operator. In this paper, we use the numerical split operator technique [20, 21], then

$$\begin{aligned} W(t+dt) &\approx e^{-iHdt} W(t) \\ &= e^{-i\frac{dt}{2} H_\partial} e^{-idt H_z} e^{-i\frac{dt}{2} H_\partial} + O(dt^3), \end{aligned} \quad (8)$$

with

$$H_\partial = c\sigma_1 \cdot \hat{p}_z + c^2\sigma_3, \quad (9)$$

$$H_z = V(z, t). \quad (10)$$

Practically, since the derivation (the momentum operator) can be implemented by replacing the operator  $\hat{p}_z$  with its value  $k_z$  in momentum space, the evolution operation has the following form

$$e^{-i\frac{dt}{2}H_\partial}W(t) = \mathcal{F}^{-1} \left[ \cos(\phi) - i \sin(\phi) \frac{\sigma_1 \cdot k_z + c\sigma_3}{\sqrt{c^2 + k_z^2}} \right] \mathcal{F}W(t) \quad (11)$$

$$e^{-idtH_z}W(t) = [\cos(V(t)dt) - i \sin(V(t)dt)]W(t), \quad (12)$$

where  $k_z$  is momentum,  $\phi = \frac{cdt}{2}\sqrt{c^2 + k_z^2}$ , and  $\mathcal{F}$  ( $\mathcal{F}^{-1}$ ) is Fourier transformation (inverse Fourier transformation).

Then, after the time dependent field operator  $\hat{\Psi}(z, t)$  can be calculated, the number, the spacial distribution of electrons created from the vacuum (defined as  $\hat{b}_p|vac\rangle = 0$ ,  $\hat{d}_n|vac\rangle = 0$ ) are obtained from the positive part of the field operator,

$$N^{el.}(t) = \langle vac | \hat{\Psi}^{(+)\dagger}(x, t) \hat{\Psi}^{(+)}(x, t) | vac \rangle = \sum_{pn} |U_{pn}(t)|^2, \quad (13)$$

$$N_z^{el.}(t) = \sum_n \left| \sum_p U_{pn}(t) W_p(z) \right|^2, \quad (14)$$

where  $U_{pn}(t) = \langle W_p(z) | W_n(z, t) \rangle = \int dx W_p^*(z) W_n(z, t)$ . The pair number  $N(t)$  is equal to the electron number  $N^{el.}(t)$ .

The spacial distribution of the created positrons can be written as

$$N_z^{po.}(t) = \sum_p \left| \sum_n U_{pn}(t) W_n(z) \right|^2. \quad (15)$$

The total positron number  $N^{po.}(t)$  is equal to the electron number  $N^{el.}(t)$ .

We can also get it from the negative part of the field operator by compute the number and spacial distribution of the holes. In this paper we use this expression (Eq. (15)) to reduce the computational cost, because  $U_{pn}$  has been calculated in Eq.(13). Furthermore, we can neglect the larger part of the momentum ( $\sqrt{k^2c^2 + c^4}$  is far greater than  $V$  and  $\omega$ ) in the numerical simulation, for its contribution to the matrix element  $U_{pn}(t)$  is very small. In the following, the number of spatial points is  $N_z = 2048$ , and we only take  $N_p = 1024$  discrete momentum into account.

Based on the projection of the field operator onto the the field-free electronic states in this method and the definition of electron and positron in the Dirac hole theory, in this paper we will present physical quantities for all time and focus on the moments when the field is absent.

### III. PUMP ELECTRON-POSITRON PAIRS FROM THE WELL POTENTIAL

For a well potential of depth  $V_0$ , if  $V_0 < 2c^2$ , the positive continuum and negative continuum can not overlap. But for a super-critical depth,  $V_0 > 2c^2$ , the domain  $c^2 - V_0 < E < -c^2$  exist, and bound states in the well are possible (which we call 'bound states embedded in the negative continuum'): their wave function do not decrease exponentially out the well, but join a continuum wave of the same energy  $E < -c^2$  out the well, hence the wave function has a non-zero probability outside. An empty bound state will spontaneously be occupied by an electron (two, if the spin is considered) from the filled Dirac sea, and the hole (identified as positron) will travel away from the well to infinity [34]. This is the picture of spontaneous creation of electron-positron pair. For a static well potential, electrons will fill the embedded bound states, and the Pauli principle will prevent further pair creation. The number of pair created should be the number of bound states which meet these conditions.

For a time dependent potential, the situation is more complicated. In paper [28], the effect of open and close a pair-creation channel was studied. The well depth is fixed at  $V_0 = 2.53c^2$ , while the width  $W$  varies between  $W_1 = 4.55\lambda_C$  and  $W_2 = 6.15\lambda_C$ . For  $W = 4.55\lambda_C$ , there is one bound state embedded in the Dirac sea, and there are two for  $W = 6.15\lambda_C$ . After enough time for saturation, the pair number will increase as one more channel is opened, but do not decrease as one of the two channels is closed. The reason is that the annihilation of the pair need the electron and positron to be in the same place, which is not satisfied because the electron remains in the well while the positrons have left the creation zone and escaped to the opposite direction.

Naturally, one can propose that if the channel is opened and closed periodically, can this mechanism will lead to a continuously pair creation? Moreover, for fixed  $W$  and varying  $V_0$ , since the diving behavior is similar (Fig. 1), will something similar happen? Motivated by these questions, we construct two oscillating modes as described in Sec. II. A. Results and discussion are as follows.

#### A. time evolution of pair number

Using the method presented in Sec. II. B, we graph the time evolution of the pair number defined as Eq.(13) for both W-oscillating and V-oscillating mode in Fig. 2. The width frequency  $\omega_W$  and depth frequency  $\omega_V$  are in units of  $c^2$ , and their values are assumed to be relative low, comparing to the gap  $2c^2$ , so that the photon absorption mechanism is not valid. The total time is  $120\pi/c^2 \approx 0.02$  and the period is  $T_W = 2\pi/\omega_W$  or  $T_V = 2\pi/\omega_V$ . The dot line represent the time  $t \approx L/(2c) \approx 0.009$  when the particles arrive the boundary,  $z = \pm L/2 = \pm 1.25$ . Since  $W_1 = 0$  and  $V_1 = 0$ , if the time is an integer multiples of

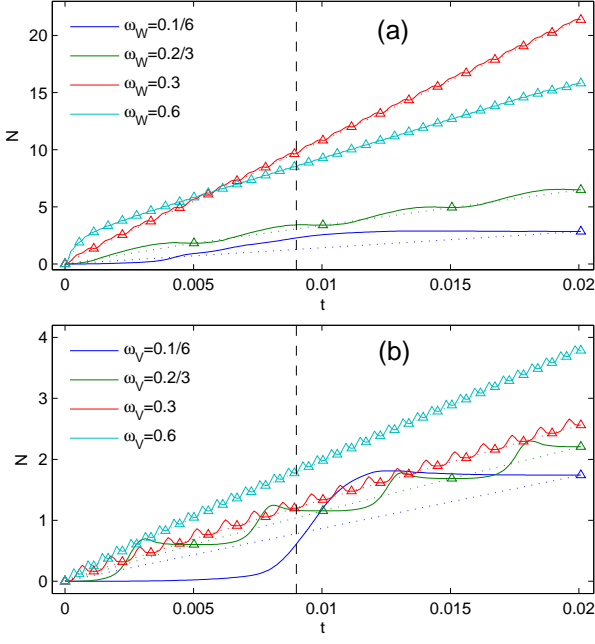


Figure 2. The time evolution of the total number of pairs for both W-oscillating and V-oscillating mode. (a), W-oscillating mode,  $W_2 = 10\lambda_C, V_0 = 2.53c^2$ ; (b), V-oscillating mode,  $V_2 = 2.53c^2, W = 10\lambda_C$ . The frequency  $\omega_W$  and  $\omega_V$  are in units of  $c^2$ . The dash line represent the time  $t = 0.009$  when the positrons arrive the boundary,  $z = \pm L/2 = \pm 1.25$ . The triangles denote pair number when the field is absent. The dot line just link these triangles.

the period ( $T_W$  or  $T_V$ ), the system Hamiltonian degenerate to a field free one. The triangles in Fig. 2 denote the pair number when the field is absent.

**W-oscillating mode:** In Fig. 2 (a), we illuminate the total number of pairs as a function of time for  $\omega_W = 0.1/6c^2, 0.2/3c^2, 0.3c^2, 0.6c^2$ . The depth  $V_0$  is fixed at  $V_0 = 2.53c^2$ . The width  $W$  varies between  $W_1 = 0$  and  $W_2 = 10\lambda_C$ , corresponding zero and three bound states embedded. When  $W = W_2$ , there are also eight bound states exist in the gap, which can be associate with the pair creation[27].

When  $\omega_W = 0.1/6c^2$ , the width  $W$  can only finish one cycle in the total time  $120\pi/c^2$ .  $N$  begin to arise before  $t = 3.57 \times 10^{-3}$ , corresponding  $W(t) = 2.79\lambda_C$ , when the first bound state dive into the negative continuum. The reason is the non-adiabatic varying width, and  $N$  will begin to arise precisely at the time when  $W(t) = 2.79\lambda_C$  in the adiabatic case ( $\omega_W \rightarrow 0$ , see the discussion below).  $N$  increases as more bound states dive in, and reach its maximum  $N = 2.89$  at  $t = 1.37 \times 10^{-2}$ , between  $t = 1.28 \times 10^{-2}$  and  $1.47 \times 10^{-2}$ , at which time the third and the second bound state were pulled out the Dirac sea. Undergoing the particle-antiparticle annihilation,  $N$  decreases but remains an appreciable value  $N = 2.85$  at the end. In the latter half of this cycle, the embedded bound states depart from the Dirac sea, return to the positive

continuum, and become scattering states. The released positrons are reflected by the numerical box boundary, come back to the interaction region and will affect the pair generation after. Though the effect is weak when  $\omega_W = 0.1/6c^2$ , it is non-ignorable when, i.e.,  $\omega_W = 0.3c^2$  (see Fig. 3 for details).

For  $\omega_W = 0.2/3c^2$  and  $\omega_W = 0.3c^2$ ,  $W$  can finish four and eighteen cycles in the total time and the pair number are  $N = 6.49, N = 21.4$  at the end. For  $t < 0.009$ ,  $W$  can finish one and eight cycles, respectively. In each cycle, the positrons are repulsed by the electric field to the infinity once they were generated, while the electrons are limited in the well when the field is strong enough and extruded out as the well is turning off, avoiding the inevitable Pauli block in the non-varied static well construction. The non-synchronous ejection prevent the annihilation and lead to a high production rate.

The next cycle starts from field free and is independent on the previous cycle. In Fig. 2, the dot line link the triangles which denote the pair number when the field is absent. We can find that the pair generation denoted by the dot line is linearly depend on time for low frequency  $\omega_W$ , for  $t < 0.009$ . If the system length  $L$  is infinite and there is no reflection at the boundary, the pairs can be pumped inexhaustibly with a constant production rate from the well. Even for  $\omega_W = 0.6c^2$ , there is nonlinear effect at the beginning, the generation rate become stable soon.

Due to the finite period  $T_W$  and the bound states in the gap, particle generation and ejection process is not monotonic with the increase of the frequency  $\omega_W$ , see Fig. 2 (a), However, ignoring the reflection, if the W-oscillating frequency  $\omega_W$  is very small, we can expect a linear dependent of final pair number on the frequency.

**V-oscillating mode:** The number of pairs  $N$  as a function of time are presented in Fig. 2 (b), for  $\omega_V = 0.1/6c^2, 0.2/3c^2, 0.3c^2$  and  $0.6c^2$ . The width  $W$  is fixed at  $W = 10\lambda_C$ , while the depth varies between  $V_1 = 0$  and  $V_2 = 2.53c^2$ , corresponding zero and three bound states embedded. There are also eight bound states exist in the gap when  $V_0 = V_2$ .

For  $\omega_W = 0.1/6c^2$ , the first bound state dive in at  $t = 7.20 \times 10^{-3}$ , at which time there are already  $N = 8.83 \times 10^{-2}$  pair generated. The first bound state depart the negative continuum after the second and the third one, at  $t = 1.29 \times 10^{-2}$ , when  $N$  reach its maximum  $N = 1.81$ . Finally, there are  $N = 1.74$  pairs survived at  $t = 120\pi/c^2$ . For  $\omega_V = 0.2/3c^2, 0.3c^2, 0.6c^2$ , the pair number at the end are  $N = 2.21, 2.56, 3.78$ .

Instead of pulling and pushing the walls of the well in W-oscillating mode, in this mode it is the rising and falling bottom of the well that control the bound states diving in and departing from the negative continuum. It is also the non-synchronous ejection of the positrons and electrons which dominant the pumping process.

The dot line here indicate a linear relation between the pair number and time. The final number is not monotonic depending on the frequency  $\omega_V$ , and we can also



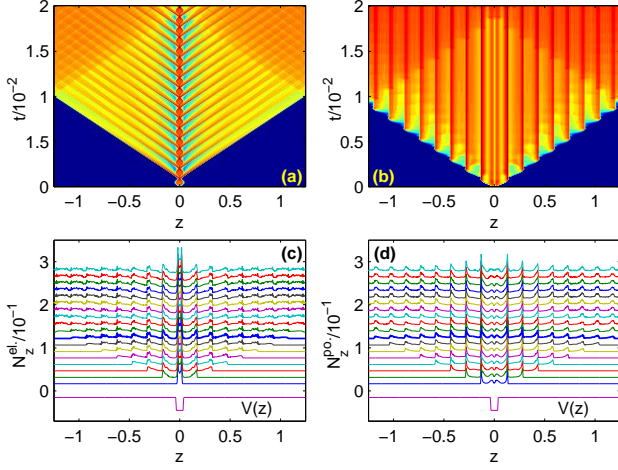


Figure 3. For W-oscillating mode,  $\omega_W = 0.3c^2$ , the three dimensional diagrams for entire time and the waterfall figures for field free moments (the time indicated by triangles in Fig. 2 (a)), for electron spacial density (a, c) and positron spacial density (b, d). The thicker curve in sub-figure (c, d) mark the last cycle before the positron arrive the boundary. The well potential  $V(z)$  with  $V_0 = 2.53c^2$ ,  $W = 10\lambda_C$ , are included on the bottom for comparison. All other parameters are the same as Fig. 2 (a).

expect a linear dependent of final pair number on  $\omega_V$  when  $\omega_V$  is very small.

Note that although the two modes has the same beginning and ending parameters, the generation rate in the W-oscillating mode is much higher.

### B. time evolution of spacial density

In last section we discussed the total pair number as a function of time in different oscillating frequency for both modes. To show the pumping process explicitly, we compute the time evolution of spacial density of electrons and positrons ( Eq. 14 and Eq.15) for  $\omega_W = 0.3c^2$  and  $\omega_V = 0.3c^2$  respectively.

In Fig. 3, for W-oscillating mode,  $\omega_W = 0.3c^2$ , we plot the the time evolution of spacial density of electrons and positrons (sub-figure (a) and (b)). Specially, for the moments when the field are zero, denoted by the triangles in Fig. 2 (a), these quantities are plotted in the waterfall figures, Fig. 3(c, d). For V-oscillating mode,  $\omega_V = 0.3c^2$ , similar diagram are presented in Fig. 4. For comparison, the well potential  $V(z)$  with wide and depth equal to the upper boundary of the two modes,  $V_0 = V_2 = 2.53c^2$ ,  $W = W_2 = 10\lambda_C$ , are included on the bottom. These figures clearly show the process how are the particles pumped from the well and spread in the numerical box.

Since  $\omega_W = 0.3c^2$ , The period of the width oscillating is  $T_W = 1.12 \times 10^{-3}$ . Before positrons arrive the boundaries, the width can finish eight cycles. If we detect the

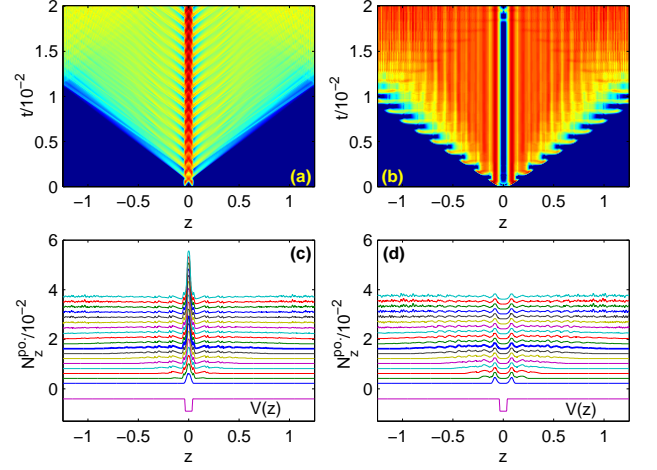


Figure 4. For V-oscillating mode,  $\omega_V = 0.3c^2$ , the three dimensional diagrams for entire time and the waterfall figures for field free moments ( the time indicated by triangles in Fig. 2 (b)), for electron spacial density (a, c) and positron spacial density (b, d). The thicker curve in sub-figure (c, d) mark the last cycle before the positron arrive the boundary. The well potential  $V(z)$  with  $V_0 = 2.53c^2$ ,  $W = 10\lambda_C$ , are included on the bottom for comparison. All other parameters are the same as Fig. 2 (b).

particle population at the boundary, we can find that positrons arrive the boundary first, at  $t = 9.15 \times 10^{-3}$ , in conformity to the estimation  $L/(2c) = 9.12 \times 10^{-3}$ . Electrons arrive the boundary at  $t = 1.02 \times 10^{-2}$ , about one period ( $T_W$  or  $T_V$ ) later than the positrons. We can see that the particles reflected by the boundary come back to the interaction region, and may cause non-ignorable effect, i.e., the non-linearity of the last three triangles in the dot line in Fig. 2(a),  $\omega_W = 0.3c^2$ .

Comparing with the rising and falling bottom of the well, more work is done by the wall of the well in the case of opening and closing the well. In the W-oscillating mode, the wavefront of the particles are more abrupter and regular. In energy space, higher energy modes are excited, and the spectrum show periodic structure with  $0.3c^2$  between each peak. In the V-oscillating mode, electrons are lifted and released naturally. Less work is done and only low momentum mode are excited, the rate of electrons in the well region ( $-5\lambda_C < z < 5\lambda_C$ ) is more larger. Also, We can see the absent of interferences both in or out the well, as discussed in [27].

### C. time evolution of pumping rate

In the V-oscillating mode, it turns out that the electrons is more inclined to gather in the well region (defined as  $-5\lambda_C < z < 5\lambda_C$ ) than it in W-oscillating mode. We can integrate the spacial density  $N(z)$  in this region and get the particle number in the well,  $N_{in}^{el.(po.)}(t) = \int_{-5\lambda_C}^{5\lambda_C} N_z^{el.(po.)}(t) dz$ . For the pumping pro-

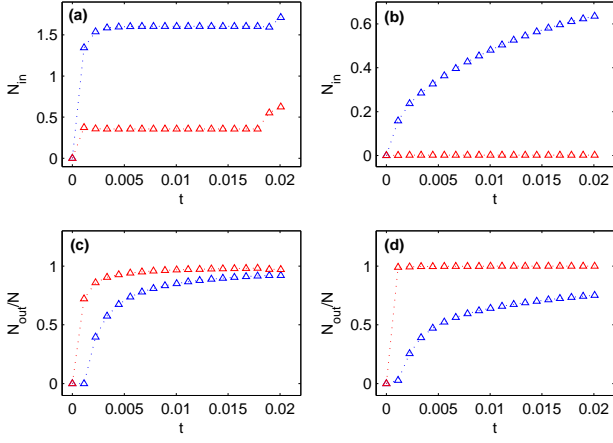


Figure 5. For W-oscillating mode ( $\omega_W = 0.3c^2$ , sub-figure a, c) and V-oscillating mode ( $\omega_V = 0.3c^2$ , sub-figure b, d), particles in the well ( $N_{in}$ ) and the pumping rate  $N_{out}/N$  as a function of time. The triangles denote the time when field is absent and the dot line link them. The blue triangles denote electron and the red denote positron. All parameters are the same as Fig. 3 and Fig. 4, respectively.

cess in last section,  $N_{in}^{el.(po.)}(t)$  are graphed in Fig. 5(a, b). In W-oscillating mode, as time increasing,  $N_{in}^{el.}$  increase to a constant 1.60 quickly, while  $N_{in}^{po.}$  to a constant 0.36. But in W-oscillating mode,  $N_{in}^{el.}$  keep increasing while  $N_{in}^{po.}$  keep zero. The reason is positrons can be generated in the well region in W-oscillating mode, while the wall (the electric field) shut the door upon positrons in V-oscillating mode.

In a pumping process, the pumping rate is vitally important and can be defined as  $\alpha(t) = N_{out}/N$ , where  $N_{out} = N - N_{in}$ , as shown in Fig. 5(c, d). In both modes, at the end of the first cycle, when  $t = T_W$  or  $T_V$ , nearly all the electrons are limited in the well region, while positron are ejected. In V-oscillating mode, since all the generated positrons are ejected and kept out of the well, the pump rate directly become 1. For electron in the V-oscillating mode, or electron and positron in W-oscillating mode, in the long time limit,  $\alpha(t)$  come to 1 as  $1 - \beta/t$ , where  $\beta$  depends on the saturation number of particles in the well and the number of particles can be generated in each cycle.

#### D. The adiabatic limit

In Fig. 2, for  $\omega_W = 0.1/6c^2$  and  $\omega_V = 0.1/6c^2$ , there are  $N = 2.85$  and  $N = 1.74$  pairs survived at the end  $t = 120\pi/c^2$ . We have proposed that in low frequency limit, the pairs survived finally should equal to three, the maximum number of embedded bound states swept in one cycle of each mode. In Fig. 6, ignoring the reflection, for each frequency, the total time is chosen equal to the oscillating period for both modes, so that the oscillation can only finish one cycle. The final number of

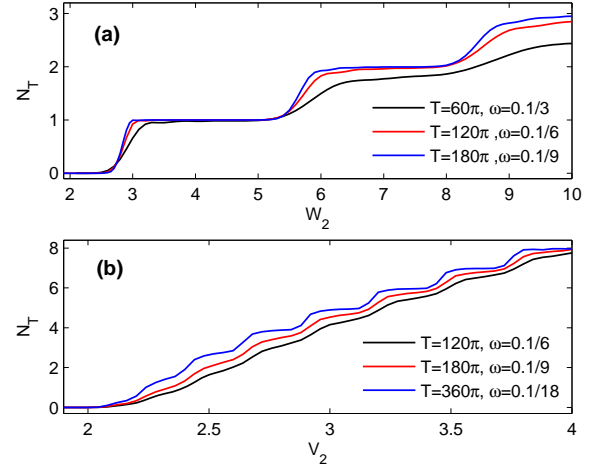


Figure 6. The final number of pairs created after one cycle as a function of the upper boundary of the oscillating width and depth. (a), W-oscillating mode,  $V_0 = 2.53c^2$ ; (b), V-oscillating mode,  $W = 10\lambda_C$ . The total time  $T$  is chosen equal to the oscillating period.  $W_2$  is in units of  $\lambda_C$ ,  $T$  is in units of  $1/c^2$ ,  $\omega$  and  $V_2$  is in units of  $c^2$ .

pairs survived as a function of the upper boundary of the oscillating width ( $W_2$ ) and depth ( $V_2$ ) are presented.

In the adiabatic limit, a sub-critical well potential can not trigger pairs. As the width or depth increasing, the bound states in the gap dive into the negative continuum successively, the potential become super-critical. Pairs can be generated and saturated to the number of embedded bound states. However, as the width and depth decreasing, bound states depart the negative continuum successively and the generated pairs can not annihilate because of the non-synchronous ejection. Finally, the number of pairs survived in this cycle is equal to the maximum number of bound states embedded. This maximum number is a function of the upper boundary of the two oscillating cycle ( $W_2$  or  $V_2$ ).

For a low frequency, the curve which indicate the final number of pairs vs.  $W_2$  or  $V_2$  is like a flight of stairs. As the frequency become lower, the rising edge of the stairs become more sharper. As shown in Fig. 6, in the limit  $\omega_W, \omega_V \rightarrow 0$ , the the rising edge of the stairs will precisely locate at the points where the bound states dive into the negative continuum. These points are  $W = 2.79, 5.51, 8.21...$ (in units of  $\lambda_C$ ), and  $V_0 = 2.05, 2.19, 2.38, 2.62, 2.87, 3.15, 3.43, 3.73, ...$ (in units of  $c^2$ ), as illuminated in Fig. 1.

The gaps between bound states in the positive and negative continuum in V-oscillating mode are smaller than that in W-oscillating mode. To achieve a quasi-adiabatic (finite  $T_W$  or  $T_V$ ) simulation,  $T_V$  should be larger than  $T_W$  to build a similar stairs.

Now, if the two quasi-adiabatic oscillating cycle repeat periodically, we can expect a linear increasing pair number, i.e., for Fig. 6(a),  $W_2 = 7\lambda_C$ , the final pair number will be 2 times the number of the cycles.

#### IV. SUMMARY

In this work, we have constructed a toy model, one-dimensional well potential with its width and depth oscillating, and studied the electron-positron creation. Since the bound states diving behavior in the energy spectrum are similar when sweeping the depth or width, the physical process are similar in these two modes. We find that the non-synchronous ejection of particles prevent the particle annihilation, break the Pauli block effect in a static super-critical well potential, and lead to a high constant production rate. The width oscillating mode can deliver more energy to particles and is more efficient in pumping pairs than the depth oscillating mode. The time evolution of spacial density illustrate the particles pumping from the well and the spreading of them in the numerical box. In a quasi-adiabatic case, pair number as a function of upper boundary of the oscillating, will reveal the diving of the bound states. This can be expected to detect the energy structure of a complicated potential.

In order to reduce the computing cost, we neglect the larger part of the discrete momentum in the numerical

simulation. On the other hand, with the same number of discrete momentum, the number of spatial points can be larger to describe the details of the potential. The simulation in this paper is done on a personal stand-alone computer. In this algorithm, the time evolution of each negative eigenstate can be done on a single CPU, hence the computation can be paralleled easily. Further more, if the second order spatial derivative in the Hamiltonian are done by finite difference approximations instead of Fourier transformation[22], more lager one-dimensional, even two dimensional system can be simulated through paralleling the algorithm on memory shared parallel computers.

#### ACKNOWLEDGMENTS

This work is supported by National Basic Research Program of China (973 Program) (Grants No. 2013CBA01502, No. 2011CB921503, and No. 2013CB834100), the National Natural Science Foundation of China (Grants No. 11374040, No. 11274051, and 11475027).

- 
- [1] Dirac, P. A. M., Proc. R. Soc. A **117**, 610 (1928).
  - [2] A. Di Piazza, C. Müller, K. Z. Hatsagortsyan, and C. H. Keitel, Rev. Mod. Phys. **84**, 1177 (2012).
  - [3] Breit, G., and J. A. Wheeler, 1934, Phys. Rev. **46**, 1087.
  - [4] F. Sauter, Z. Phys. **69**, 742 (1931).
  - [5] W. Heisenberg and H. Euler, Z. Phys. **98**, 714 (1936).
  - [6] J. Schwinger, Phys. Rev. **82**, 664 (1951).
  - [7] Brezin, E., and C. Itzykson, Phys. Rev. D **2**, 1191 (1970).
  - [8] Popov, V. S., JETP Lett. **13**, 185 (1971).
  - [9] Popov, V. S., Sov. Phys. JETP **34**, 709 (1972).
  - [10] J. C. R. Bloch, V. A. Mizerny, A. V. Prozorkevich, C. D. Roberts, S. M. Schmidt, S. A. Smolyansky, and D. V. Vinnik, Phys. Rev. D **60**, 116011 (1999).
  - [11] R. Alkofer, M. B. Hecht, C. D. Roberts, S. M. Schmidt, and D. V. Vinnik, Phys. Rev. Lett. **87**, 193902 (2001).
  - [12] Salamin, Y. I., S. X. Hu, K. Z. Hatsagortsyan, and C. H. Keitel, Phys. Rep. **427**, 41 (2006).
  - [13] C. C. Gerry, Q. Su, and R. Grobe, Phys. Rev. A **74**, 044103 (2006).
  - [14] Q. Su and R. Grobe, Laser Phys. **17**, 92 (2007).
  - [15] T. Cheng, Q. Su, and R. Grobe, Phys. Rev. A **80**, 013410 (2009).
  - [16] G. R. Mocken, M. Ruf, C. Müller, and C. H. Keitel, Phys. Rev. A **81**, 022122 (2010).
  - [17] M. Jiang, W. Su, Z. Q. Lv, X. Lu, Y. J. Li, R. Grobe, and Q. Su, Phys. Rev. A **85**, 033408 (2012).
  - [18] A. Belkacem et al., Phys. Rev. Lett. **71**, 1514 (1993).
  - [19] D. L. Burke, R. C. Field, G. Horton-Smith, J. E. Spencer, D. Walz, S. C. Berridge, W. M. Bugg, K. Shmakov, A. W. Weidemann, C. Bula, K. T. McDonald, E. J. Prebys, C. Bamber, S. J. Boege, T. Koffas, T. Kotseroglou, A. C. Melissinos, D. D. Meyerhofer, D. A. Reis, and W. Ragg, Phys. Rev. Lett. **79**, 1626 (1997).
  - [20] G. R. Mocken and C. H. Keitel, J. Comput. Phys. **199**, 558 (2004).
  - [21] G. R. Mocken and C. H. Keitel, Comput. Phys. Commun. **178**, 868 (2008).
  - [22] M. Ruf, H. Bauke, and C. H. Keitel, J. Comp. Phys. **228**, 9092 (2009).
  - [23] P. Krekora, Q. Su, and R. Grobe, Phys. Rev. Lett. **92**, 040406 (2004).
  - [24] P. Krekora, Q. Su, and R. Grobe, Phys. Rev. A **72**, 064103 (2005).
  - [25] P. Krekora, Q. Su, and R. Grobe, Phys. Rev. Lett. **93**, 043004 (2004).
  - [26] Christopher C. Gerry, Q. Su, and R. Grobe, Phys. Rev. A **74**, 044103 (2006).
  - [27] P. Krekora, K. Cooley, Q. Su, and R. Grobe, Phys. Rev. Lett. **95**, 070403 (2005).
  - [28] Y. Liu, M. Jiang, Q. Z. Lv, Y. T. Li, R. Grobe, and Q. Su, Phys. Rev. A **89**, 012127 (2014).
  - [29] Suo Tang, Bai-Song Xie, Ding Lu, Hong-Yu Wang, Li-Bin Fu, and Jie Liu, Phys. Rev. A **88**, 012106 (2013).
  - [30] C. Müller, K. Z. Hatsagortsyan, M. Ruf, S. J. Müller, H. G. Hetzheim, M. C. Kohler, and C. H. Keitel, Laser Phys. **19**, 1743 (2009).
  - [31] Cheng, Q. Su, and R. Grobe, Contemp. Phys. **51**, 315 (2010).
  - [32] M. Jiang, Q. Z. Lv, Z. M. Sheng, R. Grobe, and Q. Su, Phys. Rev. A **87**, 042503 (2013).
  - [33] Q. Z. Lv, Y. Liu, Y. J. Li, R. Grobe, and Q. Su, Phys. Rev. A **90**, 013405 (2014).
  - [34] W. Greiner, B. Müller, and J. Rafelski, Quantum Electrodynamics of Strong Fields (Springer Verlag, Berlin, 1985).
  - [35] W. Greiner, Relativistic Quantum Mechanics, 3rd ed. (Springer, Berlin, 2000);